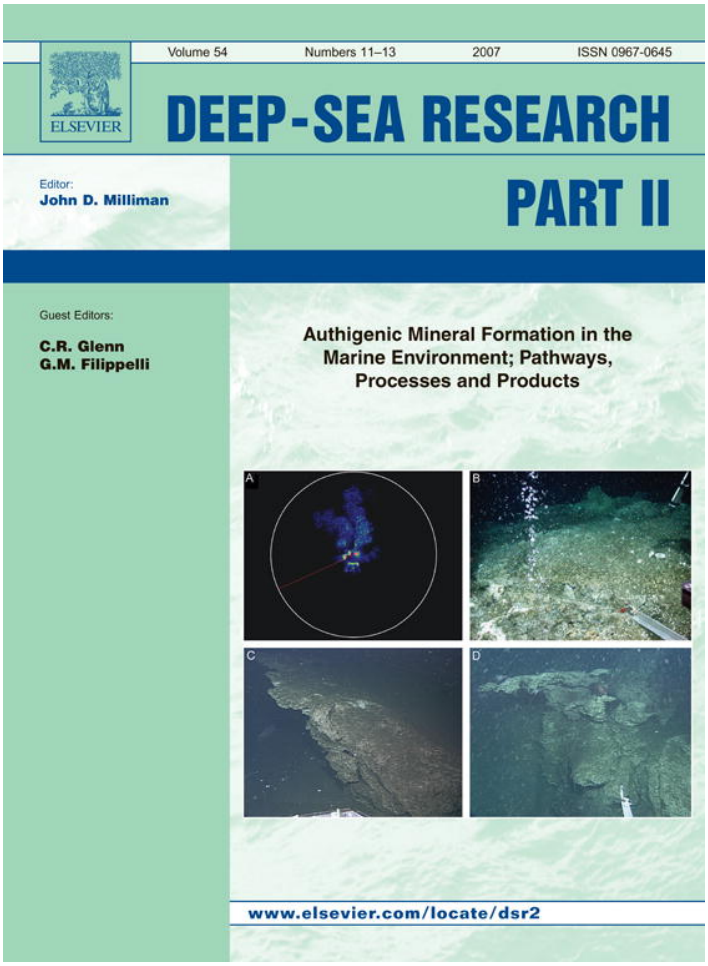

Available online at www.sciencedirect.com
ScienceDirect
ELSEVIER
Deep-Sea Research II 54 (2007) 1414–1432
DEEP-SEA RESEARCH PART II
www.elsevier.com/locate/dsr2

Geochemistry of rare earth elements in early-diagenetic miocene phosphatic concretions of Patagonia, Argentina: Phosphogenetic implications

A.M. Fazio[a,*], R.A. Scasso[a], L.N. Castro[a], S. Carey[b]

[a]*Departamento de Ciencias Geológicas, Facultad de Ciencias Exactas y Naturales, Universidad de Buenos Aires Ciudad Universitaria. Pab 2.1° Piso. 1428. Buenos Aires, Argentina*
[b]*Graduate School of Oceanography, Narragansett Bay Campus, University of Rhode Island, 02882 RI, USA*

Accepted 12 April 2007
Available online 12 July 2007

Abstract

Phosphatic concretions in the Early Miocene, shallow marine, clastic deposits of the Gaiman Formation (Gaiman Fm.) show typical major element ratios, rare earth element (REE) patterns, and total REE contents. These characteristics are similar within different stratigraphic levels and geographic locations of the unit in central-north Patagonia, Argentina and suggest a common process for the origin of the concretions. Major element oxides in concretions are grouped into a "clastic" group (Si, Al, Ti, K and Fe), that mostly corresponds to the silicates in the terrigenous fraction, and an "authigenic" group (P, Ca and total REEs), that corresponds to authigenic francolite and calcite. Mn is the only element that exhibits a separate behavior, most likely because of its high mobility in seawater. Major element ratios in host shales are similar to those of the clastic fraction within the concretions and coquinas. Concretions are slightly depleted in LREEs and slightly enriched in HREEs in comparison to shales and display a weak negative Ce anomaly. Their La/Yb and La/Sm ratios indicate REEs incorporation from pore water without strong postdepositional recrystallization or strong adsorption. Y anomalies and La/Nd ratios in concretions are equivalent to seawater or slightly lower, suggesting that Gaiman concretions did not undergo intense diagenesis, but they were probably formed from phosphatic solutions impoverished in Y and La as a result of REEs release to solution from organic complexes in the early diagenesis. Flat, linear REE patterns also support an early-diagenetic origin for the concretions, via quantitative precipitation of phosphate from oxic–suboxic pore waters. Water circulation through burrows at the Miocene seawater–sediment interface improved ion diffusion and pore water renewal in the sediments, allowing the development of a widened early-diagenetic oxic–suboxic zone and the precipitation of phosphate with a homogeneous REE pattern.

Keywords: Rare earth elements; Phosphogenesis; Concretions; Phosphate; Miocene; Patagonia; Argentina

1. Introduction

The abundance and distribution patterns of rare earth elements (REEs) in phosphorites reflect the source and the mechanism of their incorporation. Phosphate material frequently incorporates REEs either directly or indirectly from seawater, by remobilization from suspended material in the water column stay as is, associated detritic material or/and, ferromanganese oxides or/and biological debris (Elderfield and Greaves, 1982; Elderfield et al.,

*Corresponding author. Fax: +54 11 4576 3329.
E-mail address: amfazio@gl.fcen.uba.ar (A.M. Fazio).

0967-0645/$ - see front matter © 2007 Elsevier Ltd. All rights reserved.
doi:10.1016/j.dsr2.2007.04.013

1981; Kolodny, 1981; McArthur and Walsh, 1984; Glenn et al., 1994 and Jarvis et al., 1994). In spite of the low REE seawater contents (less than 100 ppm of total REEs), the long residence time of the sediments at the seafloor environment promotes the active ionic exchange and the consequent REE enrichment. As indicated by many authors (McArthur and Walsh, 1984; Jarvis et al., 1994, among others), REE geochemistry of phosphorites provides an interesting tool to understand the depositional environment, because different REE patterns are observed in different marine depositional settings. Moreover, recent work by Haley et al. (2004) demonstrated that pore waters can acquire characteristic REE patterns in different early-diagenetic environments. The original REE seawater pattern in sediments and its abundance can, however, be modified by weathering, burial diagenesis, and metamorphism (McArthur and Walsh, 1984).

Phosphatic concretions formed in the Miocene shallow marine environments of Patagonia (Scasso and Castro, 1999) exhibit distinctive REE patterns that have been only partially studied (Castro et al., 2000; Castro and Fazio, 2004). A rare association of fallout tuff deposits and phosphate concretion development has been found in these beds (Leanza et al., 1981; Scasso and Castro, 1999). The geochemistry, and especially the REEs, provides a useful tool to investigate the origin of the Miocene concretions under the light of new investigations in recent deposits (e.g., Haley et al., 2004).

2. Geological setting

Flat-lying Miocene rocks of the Gaiman Formation (Gaiman Fm.) reach up to 200 m of thickness along the Atlantic coast near Rawson city, and wedge out to the west along the south wall of the lower Chubut river valley, in the Provincia del Chubut, Argentina (Fig. 1). The Gaiman Fm. consists of a coarsening upwards succession of mudstones; fine tuffs, sandstones and coquinas, rich in phosphatic concretions, ray teeth, shark teeth and bones from marine vertebrates (Scasso and Castro, 1999). Whitish tuffaceous, bioturbated mudstones with occasional thin levels of *Ostrea* dominate in the lower part of the section. They may contain volcanic glass, diatoms and siliceous sponge spicules, with smectite and illite–smectite being the main clay minerals. Sandstones and tuffaceous sandstones are common in the middle and upper part of the column and show ripples and parallel or hummocky cross stratification. Large, well-preserved *Ophiomorpha* burrows are typical in this part of the section. Thin, intercalated coquinas with broken and reworked shells and calcite cement are not rare, and a phosphatic conglomerate with reworked concretions cemented by francolite, together with pebbles, broken shells, bones and teeth occurs in the upper part of the column.

Two types of phosphatic beds have been recognized in the Gaiman Fm. (Scasso and Castro, 1999). The first, "Type 1", consists of "*in situ*" elliptical–rounded to crusty–irregular concretions ranging from very coarse sand to cobble in size. Variable amounts of iron and manganese give a yellowish to gray or rusty-brown color to the concretions, in which the phosphate frequently occurs as cement in an outer rim. Concretions are typically dispersed into the mass of host sediments and the same type of sediment is found inside and outside the concretions, as in the case of some fallout tuff beds that contain concretions with shards and pumice within them. Concretions are frequently developed in burrows (Fig. 2) or around the remains of bivalves, gastropods and callianasid shrimps, and they may show evidences of encrusting and boring organisms. These deposits are interpreted as condensed sections associated with long periods of slow effective sedimentation, part of transgressive to early-highstand system tracts (Scasso and Castro, 1999). The conjunction of sedimentation rate and phosphate productivity was not effective enough to produce highly condensed beds or hardgrounds. As a result, the phosphate particles are disseminated into the sediment and they have not been remobilized.

The second type of concretions ("Type 2") is related to reworking, winnowing and mechanical concentration of resistant particles. Dark yellow to brown phosphatic concretions, together with fish bones, teeth and scales, are mixed with broken and abraded shells and pebbles of different composition, all immersed in a sandy matrix. Borings and encrusting organisms are frequently found on the surface of the concretions. Two levels with these characteristics were found in Bryn Gwyn, one at the base and the other in the upper part of the section, both considered as reworked horizons resulting from multi-event condensation processes associated with transgressive surfaces (Scasso and Castro, 1999).

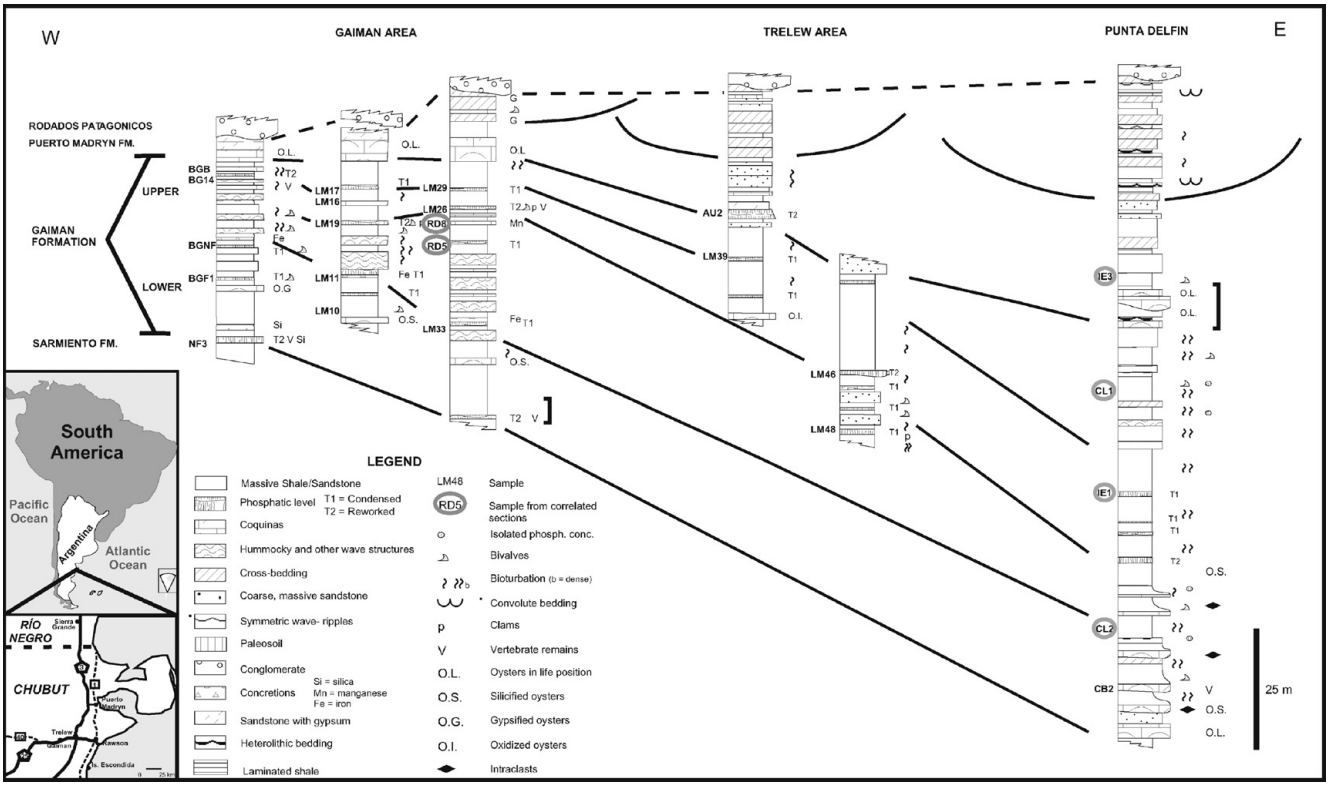

Fig. 1. Location map and cross-section of the Gaiman Formation along the lower valley of the Chubut river, showing main lithological features, name and location of the samples (modified from Scasso and Castro, 1999). Encircled samples belong to sections located to the north and to the south of the valley and their stratigraphic position is approximated by stratigraphical correlation.

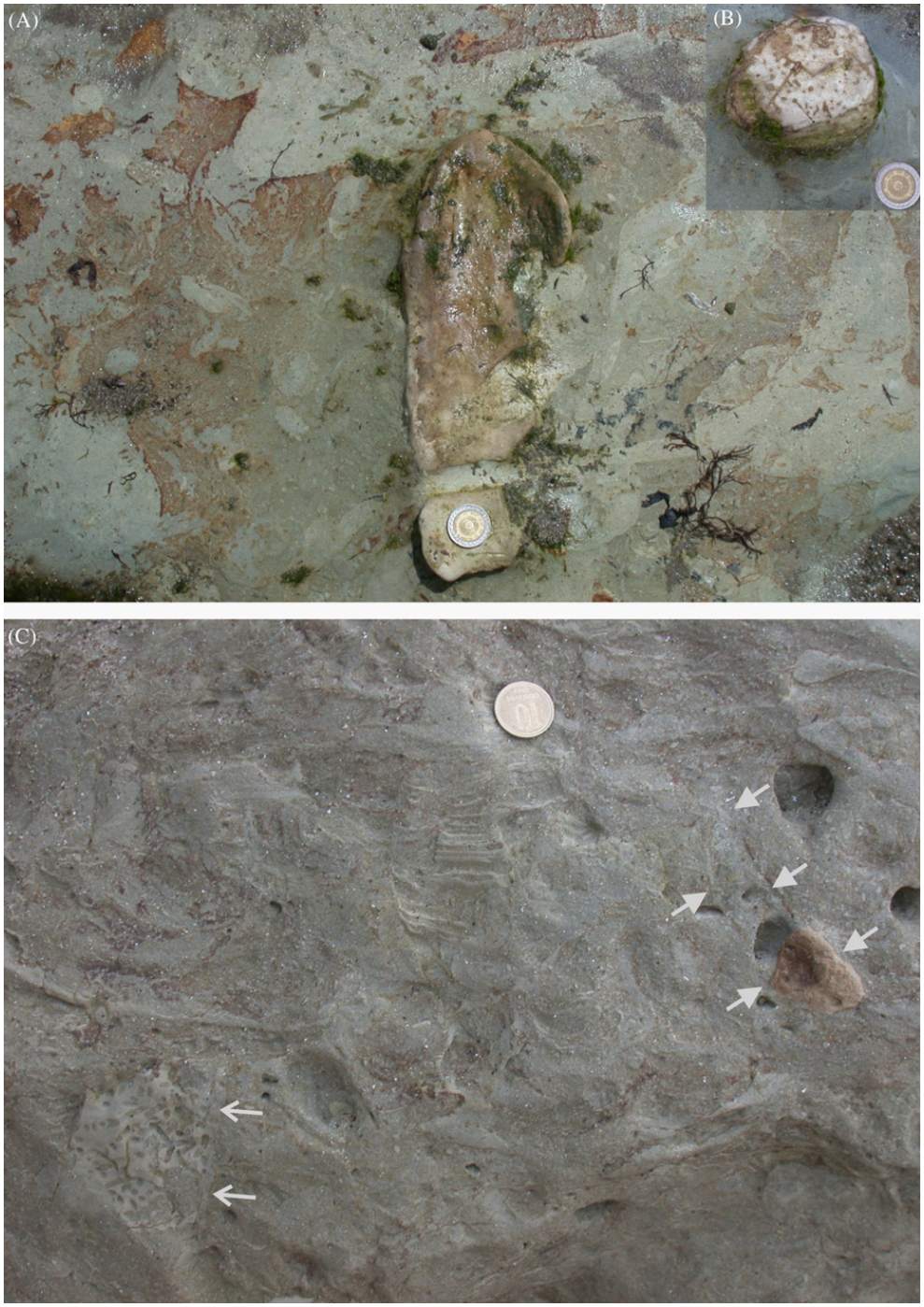

Fig. 2. (A) Part of the phosphatized wall of a large, horizontal shaft (*Thalassinoides* or *Ophiomorpha* ichnospecies) in a densely bioturbated mud. The lower part is crossed by a meniscate trace fossil developed later. Note that this part lacks phosphate cement because it was removed by the trace-maker organism before phosphate was totally indurated. (B) Section of wholly phosphatized *Thalassinoides* vertical shaft. The phosphatized infilling of the tube presents smaller trace fossils that are richer in phosphate and more indurated. Coin is 23 mm long. (C) Phosphatic concretion at the end of a subvertical trace fossil (right, arrowed). Note that sediment is completely bioturbated and only some big burrows, formed when the sediment was already buried by at least one meter of sediment, are clearly outlined. In the filling of some large burrows *Chondrites* isp., a trace fossil typical of suboxic environments, is developed in the filling of some large burrows (outline of the large burrow arrowed, lower left). Section perpendicular to the bedding plane, coin is 19 mm in diameter.

3. Methodology

The Gaiman Fm. was sampled in a wide area along the Atlantic coast of Río Negro and Chubut provinces, from Sierra Grande in the north to Isla Escondida in the south. The name, lithology and location of the samples are given in Fig. 1. Phosphates, mudstones and coquinas from different sections belonging to different stratigraphic parts of the Gaiman Fm. were sampled at many different outcrops, varying from recently exposed coastal cliffs, to older exposures inland. Paired samples of phosphate concretions and their host shales were analyzed in order to compare the REE patterns.

Petrographic composition was studied by standard optical methods and by X-ray diffraction (XRD) in the Departamento de Ciencias Geológicas, University of Buenos Aires. Polished sections were studied under the scanning electron microscopy (SEM) (JEOL JSM 5900LV) and semi-quantitative energy dispersive X-ray analysis (EDX) analyses were carried out with a PGT EDS system in the University of Rhode Island.

A 0.250 g sample of powered rock, plus 5 ml HNO_3 (c) and 10 ml of HF (c) were digested in a Milestone microwave oven in three digestion steps of 5 min each, with increasing power up to 650 kW to allow complete dissolution. The vessels were stored over night and then evaporated to incipient dryness on a hotplate at 200 °C. About 5 ml of HF (c) were added to each vessel and again evaporated. The residue was dissolved in 5 ml of HNO_3 (c) with gentle heating, until a clear solution resulted. After cooling, samples were diluted with deionized water to 50 ml in a volumetric flask. Finally, samples were stored in polypropylene bottles until the UVS, AAS and ICP–AES measurements were carried out. Aliquots of samples were taken for SiO_2, TiO_2, Fe_2O_3, and MnO determination by UV-spectrometric methods with molybdenum blue, Tyron, orthophenantrolyne and KIO_4–H_2SO_4, respectively. Simultaneous analysis of Na_2O, K_2O, CaO and MgO by AAS were performed in other aliquot of sample (Shapiro, 1975). The major constituents (Table 1) were determined in the Laboratorio de Análisis de Rocas of the Departamento de

Table 1
Chemical analysis (wt%) of phosphatic concretions and crusts, coquinas, and host shales of the Gaiman Formation

Sample	Type	SiO_2	TiO_2	Al_2O_3	Fe_2O_3	MnO_2	MgO	CaO	Na_2O	K_2O	P_2O_5	H_2O^+	H_2O^-	CO_2	Total
AU2	Concretion	29.58	0.24	6.85	2.20	0.06	0.77	29.84	2.45	1.04	16.52	1.44	1.61	6.57	99.17
BG14	Concretion	25.60	0.30	0.46	1.71	0.17	0.49	38.61	1.06	0.10	20.25	1.80	4.51	5.14	100.20
BGNF	Concretion	32.80	0.27	7.52	1.45	0.20	0.92	26.00	3.39	1.29	16.54	7.39	2.01	–	99.78
CB2	Concretion	24.50	0.33	8.91	2.80	0.05	0.96	31.96	2.24	0.75	17.43	0.97	1.79	7.70	100.39
CL1	Concretion	24.14	0.32	7.50	2.87	0.01	0.95	33.50	1.95	0.73	18.25	0.02	1.50	7.43	99.17
IE1	Concretion	37.90	0.27	5.62	1.22	0.07	0.85	26.00	3.40	1.35	14.90	6.93	2.37	–	100.88
LM10	Concretion	41.20	0.33	6.58	1.43	0.09	0.67	23.50	2.94	1.41	14.50	5.08	2.41	–	100.14
LM11	Concretion	35.50	0.26	6.37	1.63	0.05	0.99	24.74	2.20	1.31	17.57	8.14	1.69	–	100.45
LM17	Concretion	23.13	0.25	5.96	1.86	0.15	0.49	32.43	1.71	0.81	24.97	1.78	2.21	4.56	100.31
LM26	Concretion	30.70	0.35	6.86	2.82	0.04	0.70	28.90	2.29	1.21	17.92	6.07	1.78	–	99.63
LM29	Concretion	43.86	0.40	9.93	2.56	0.07	0.97	16.92	3.94	1.59	12.37	5.54	2.14	–	100.29
LM33	Concretion	32.51	0.35	7.49	3.04	0.10	0.84	27.50	2.37	1.40	16.28	6.61	1.81	–	100.30
LM46	Concretion	23.38	0.29	6.05	2.31	0.12	0.56	32.61	1.69	0.75	25.17	2.11	2.29	4.23	101.27
LM48	Concretion	42.30	0.32	6.95	1.67	0.05	0.64	18.67	3.27	1.28	11.98	6.63	1.55	5.00	100.31
NF3	Crust	30.59	0.33	12.53	2.94	0.10	1.16	24.15	2.09	1.71	17.31	4.86	1.60	–	99.38
RD8	Concretion	32.92	0.27	6.74	2.51	0.17	1.01	25.52	3.46	1.07	17.29	7.93	2.02	–	100.91
RD5	Concretion	30.84	0.25	4.28	2.20	0.16	2.30	27.77	2.20	0.88	16.87	10.38	1.32	–	99.46
IE3	Coquina	37.09	0.27	8.06	2.75	0.05	0.72	20.16	1.46	1.17	3.95	0.05	1.60	23.10	100.43
LM39	Coquina	56.21	0.54	10.04	2.53	0.10	2.24	5.40	4.79	1.62	3.88	2.76	1.64	8.02	99.76
CL2	Shale	52.43	0.69	14.10	5.10	0.04	1.74	2.63	6.22	1.93	0.50	8.14	6.40	2.76	102.67
LM16	Shale	59.68	0.59	13.50	4.50	0.04	1.33	2.18	2.36	1.88	0.29	5.16	4.90	1.80	98.21
BGB	Shale	61.95	0.36	14.60	4.70	0.04	1.18	3.50	2.15	2.14	0.43	3.52	3.85	1.81	100.23
LM19	Shale	55.43	0.59	13.38	5.50	0.01	2.41	3.51	2.46	1.87	1.25	6.54	5.52	1.05	99.52

SiO_2, TiO_2, Al_2O_3, Fe_2O_3, MnO_2 and P_2O_5 were determined by molecular absorption spectrophotometry, Na_2O, K_2O, CaO and MgO by atomic emission spectrophotometry, CO_2 by acid-base titration. Total values below 100% are due to the lack of fluorine determination.

Table 2
REE chemical analysis of phosphatic concretions, coquinas and host shales. REEs were analyzed by ICP–MS in Activation Laboratories Ltd., Ontario, Canada, and by ICP–OES in the Comisión Nacional Energía Atómica (CNEA), Argentina

Sample	Type	Y	La	Ce	Pr	Nd	Sm	Eu	Gd	Tb	Dy	Ho	Er	Tm	Yb	Lu	S REEs
Au2	Concretion	228.0	130.0	290.0	28.8	133.0	31.5	6.8	35.2	5.8	30.9	7.2	19.1	3.0	16.2	2.9	740.4
BG14	Concretion	323.0	169.0	252.0	32.7	140.0	31.0	7.1	38.0	6.7	42.0	9.3	30.0	4.5	28.0	4.5	794.8
BG-F1	Concretion	478.0	207.1	236.2	32.4	139.6	29.5	7.2	40.8	7.5	51.5	12.9	42.9	6.5	39.6	6.7	860.5
BGNF	Concretion	255.0	135.0	210.0	27.8	124.0	27.3	6.0	33.6	5.1	31.5	7.8	20.8	3.0	21.4	3.7	657.0
CB2	Concretion	338.0	123.0	225.0	19.1	93.3	21.1	5.1	28.9	4.8	35.5	8.8	27.0	3.9	28.0	5.0	628.5
CL1	Concretion	804.0	215.3	275.5	28.9	125.7	26.8	7.2	44.0	8.9	67.7	19.2	68.2	10.5	65.0	11.9	974.8
IE1	Concretion	390.0	182.0	425.0	44.2	189.0	42.9	9.8	53.8	7.9	51.1	12.2	30.9	3.9	26.7	4.5	1083.9
LM10	Concretion	448.0	120.0	270.0	24.4	111.0	29.8	7.7	48.4	7.5	57.5	13.9	39.4	5.5	36.5	6.4	778.0
LM11	Concretion	343.0	214.0	273.0	35.4	168.0	33.0	7.8	44.5	6.4	38.0	9.8	27.2	3.6	26.8	4.7	892.2
LM17	Concretion	217.0	84.0	188.6	22.0	90.5	23.9	5.8	25.0	5.1	32.5	7.1	22.5	3.5	21.8	3.4	535.5
LM26	Concretion	565.0	180.0	270.0	34.0	150.0	31.3	7.9	47.9	7.4	58.0	14.9	44.0	6.8	48.8	8.7	909.7
LM29	Concretion	269.0	101.5	145.0	14.3	52.9	13.1	3.4	20.0	3.4	23.7	6.5	20.7	2.9	21.8	4.1	433.3
LM33	Concretion	471.0	221.0	390.0	35.2	155.0	24.0	8.3	47.3	7.2	58.0	12.7	37.0	5.1	36.0	6.7	1043.5
LM46	Concretion	950.0	304.0	417.0	48.3	210.0	49.0	11.7	64.0	12.0	84.0	21.0	75.0	12.3	84.0	12.3	1404.6
LM48	Concretion	730.0	243.0	450.0	47.0	197.0	49.8	12.0	72.7	11.5	86.0	21.0	60.0	8.9	57.6	10.6	1327.1
NF3	Crust	55.0	21.0	50.8	4.2	18.7	4.5	1.4	7.0	1.3	5.5	1.5	4.5	0.8	4.8	0.8	126.7
RD5	Concretion	466.0	141.0	252.5	25.5	103.0	24.9	6.4	38.1	5.9	47.3	11.7	34.9	5.0	35.9	6.6	738.7
RD8	Concretion	280.0	170.0	286.0	25.8	120.0	26.3	5.8	32.6	4.3	31.2	7.8	23.0	3.2	23.9	4.2	764.1
IE3	Coquina	42.0	26.0	50.0	4.4	16.8	4.9	1.2	6.7	1.1	6.2	2.2	5.8	1.2	7.0	1.3	134.8
LM39	Coquina	58.0	24.0	44.0	4.8	20.0	4.7	1.3	5.5	1.1	5.0	1.3	4.1	0.8	4.5	0.7	121.8
BG-B	Shale	23.0	25.6	55.4	6.1	24.5	5.0	1.1	4.3	0.7	4.2	0.9	2.5	0.4	2.3	0.3	133.3
CL2	Shale	25.0	19.3	43.6	5.1	21.3	4.6	1.1	4.3	0.7	4.3	0.9	2.7	0.4	2.5	0.4	111.2
LM16	Shale	31.0	23.8	51.5	6.0	24.3	5.4	1.3	5.1	0.9	5.4	1.2	3.5	0.5	3.3	0.5	132.6
LM19	Shale	29.0	24.1	43.0	5.9	23.4	5.0	1.1	4.7	0.9	4.6	1.0	2.9	0.6	2.7	0.4	120.5

REE concentrations are reported in ppm and normalized to the average shale (Piper, 1974).

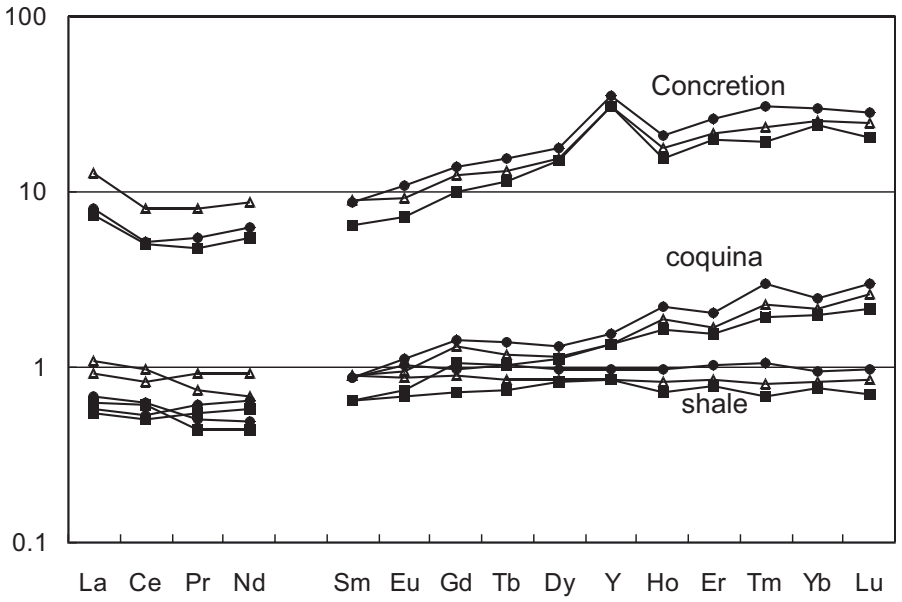

Fig. 3. Typical concretion, shale and coquina REE patterns of the Gaiman Formation normalized with different standards. Piper (Piper, 1974) average shale = full squares; PAAS (McLennan, 1989) = full circles; local host shale RB19 = empty triangles. Patterns are similar for the different standards.

Geología, Facultad de Ciencias Exactas y Naturales, Universidad de Buenos Aires.

Trace elements were analyzed by ICP–MS in Activation laboratories LTD, Ontario, Canada and by ICP–OES in the Comisión Nacional Energía Atómica (CNEA, Argentina. REE concentrations are reported in parts per million (Table 2). Normalization of REEs data by the PAAS average shale (McLennan, 1989), Piper average shale (Piper, 1974), and our local host shale revealed no significant differences (Fig. 3). We used Piper average shale because it is a compilation of worldwide shale data (Piper, 1974). The different anomalies and parameters to evaluate the REE behavior are expressed as follows:

$$\text{Anom Ce} = 3\text{Ce}_N/(2\text{La}_N + \text{Nd}_N),$$

$$\text{Anom Y} = 2\text{Y}_N/(\text{Dy}_N + \text{Ho}_N).$$

Lanthanum anomaly is expressed as La/Nd ratio. Light REE enrichment is expressed as La_n/Yb_n and La_n/Sm_n which resemble concave down-shape pattern.

Factor analyses by principal components were carried out taking as variables major elements, REEs and some selected parameters (Y and Ce anomalies and La/Nd ratio).

4. Results

4.1. Mineral composition

The phosphate is mainly presented as a cement in pores, bonding organic-phosphatic and non-phosphatic (detritic or pyroclastic) particles (Fig. 4), as a filling in pumice vesicles (Fig. 5) or as a diagenetic replacement of glassy shards and other original components of the rock (Figs. 4 and 5). It is formed by tiny crystals less than 3 μm and very regular in size, identified as a mixture of fluorapatite and carbonate–hydroxyapatite by XRD. Dark to brown colored samples showed some additional "peaks" typical of iron-rich phosphates, but not enough for confident mineral identification. Calcite and ferroan dolomite occasionally form an outer rim to the phosphatic nucleus of the concretions.

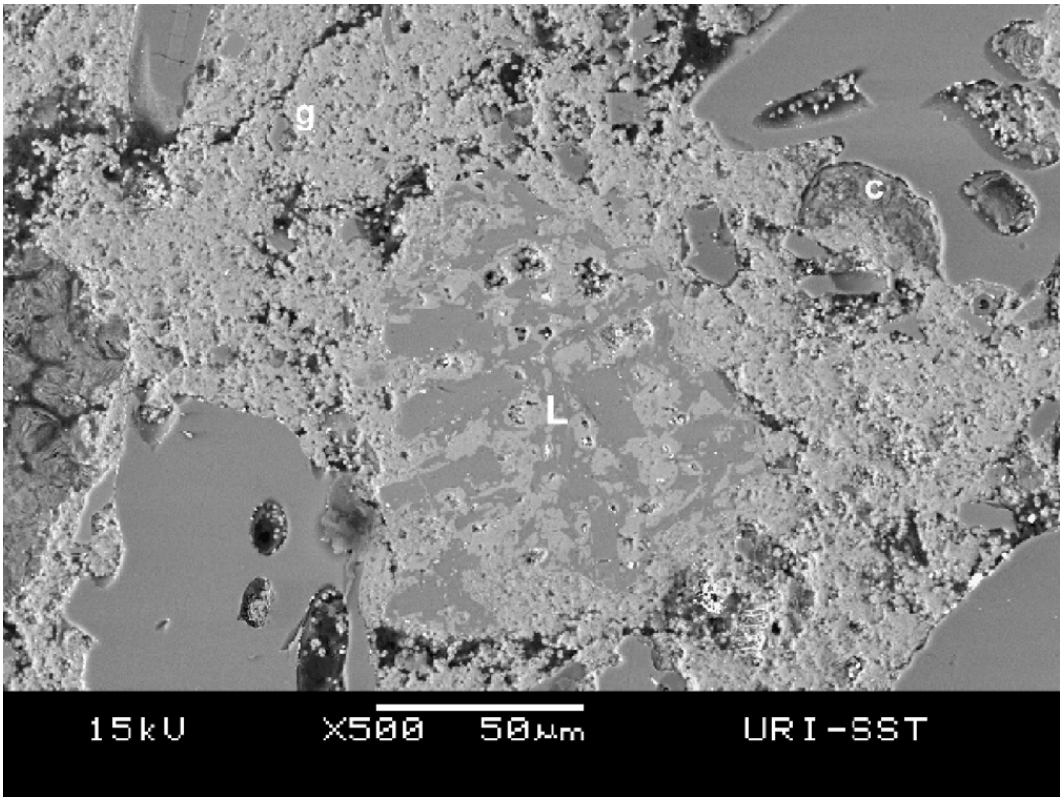

Fig. 4. Back-scattered SEM picture of a glass shards and lithic fragments in phosphatic matrix. Tiny francolite crystals of similar size make up most of the background and grow inside the vesicles. Francolite also replaces part of a lithic fragment (L) and most of the matrix, where some small glass particles (g) still remain. Part of the vesicles are filled with clay minerals (c).

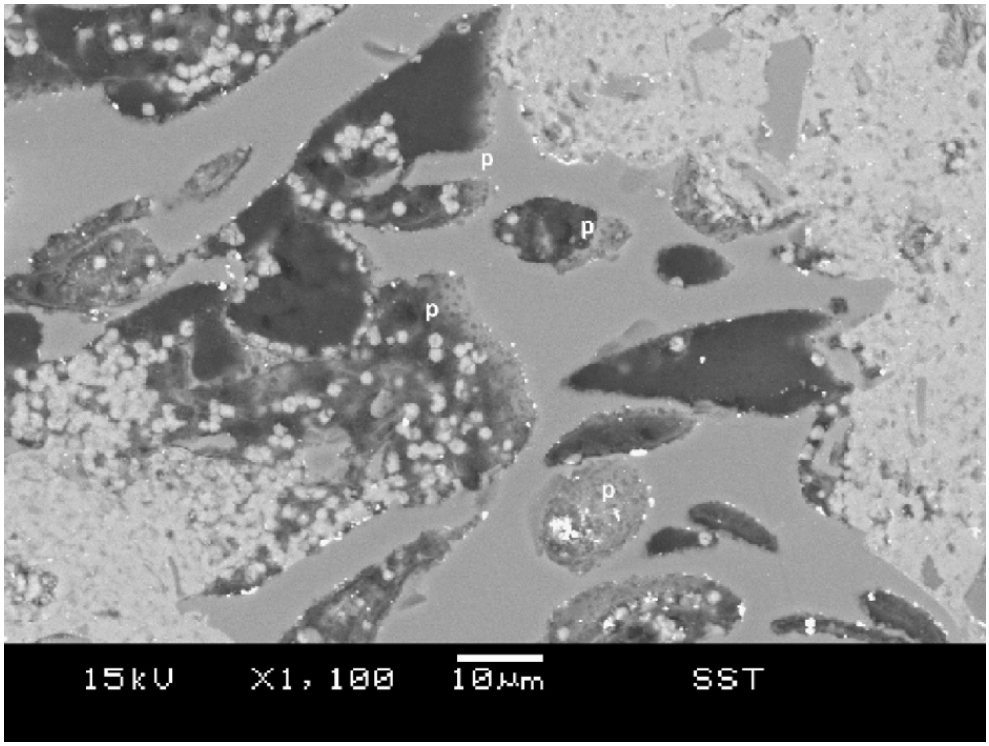

Fig. 5. Back-scattered SEM picture of a glass fragment with vesicles partially filled with small francolite crystals. Glass outlines look corroded and partially dissolved with some pitting (p).

4.2. Major elements

Phosphatic concretions show high P_2O_5 content (between 15.6% and 21.82%) and similar bulk compositions (Table 1). Phosphatic concretions are rich in oxides predominantly incorporated in the apatite lattice (CaO, Na_2O, P_2O_5 and CO_2). Coquinas show high CaO and CO_2 contents with considerable amounts of P_2O_5 from reworked concretions, and shales are rich in oxides typical from detritic and pyroclastic materials like quartz, feldspar, iron oxides, clay minerals, volcanic glass, biotite and pyroxene (SiO_2, TiO_2, Al_2O_3, Fe_2O_3, MnO, MgO, K_2O). This is reflected in the correlation matrix of Table 3, in which the two groups, named here "authigenic" and "clastic" (see below), clearly arise from the correlation coefficients. A plot of Fe_2O_3/TiO_2 vs. $Al_2O_3/Al_2O_3+Fe_2O_3$ (Fig. 6) shows that samples from coquinas, shales and concretions are tightly grouped.

4.3. Rare earth elements (REEs)

REE and Y contents in Gaiman Formation phosphates average 800 and 287 $\mu g\,g^{-1}$, respectively, higher than those of the average phosphorite, which are 462 $\mu g\,g^{-1}$ for REEs and 275 $\mu g\,g^{-1}$ for Y (Altschuler, 1980).

Shale-normalized REE patterns grouped in concretions, host shales, and coquinas show different shapes (Fig. 7). Phosphatic concretions (Fig. 7A) show a pattern roughly similar to seawater (Goldberg et al., 1963; Altschuler et al., 1967), which is depleted in light REEs (LREEs) and enriched in heavy REEs (HREEs) in comparison with shales. All phosphate concretions display a weak negative Ce anomaly, qualitatively described in this paper as the "V" defined by La, Ce and Pr. Phosphatic samples from different stratigraphic levels in the Gaiman Fm. and from several sections in different geographic locations show remarkably similar REE patterns and total contents. No differences between Types 1 (*in situ*) and 2 (reworked) concretions were found.

Host shales exhibit a typical flat pattern (Fig. 7B) with total REE contents slightly lower than Piper reference shale (Piper, 1974). Coquinas contain reworked concretions that make up to 5% P_2O_5 in the bulk composition. Consequently they display patterns similar to the concretions (Fig. 7C), but with lower total REE contents (about 128 $\mu g\,g^{-1}$).

Table 3
Correlation matrix

	ΣREEs	CaO	P_2O_5	Al_2O_3	TiO_2	Fe_2O_3	K_2O	SIO_2	MnO	MgO	Na_2O
ΣREEs	1.0000	0.6860	0.7116	−0.7146	−0.5858	−0.6370	−0.5863	−0.6083	0.1948	−0.5407	−0.2386
CaO		1.0000	0.9319	−0.8352	−0.8118	−0.7230	−0.8791	−0.9683	0.4433	−0.6273	−0.5430
P_2O_5			1.0000	−0.7551	−0.7504	−0.7204	−0.7684	−0.9212	0.5181	−0.5748	−0.4350
Al_2O_3				1.0000	0.7196	0.8226	0.8702	0.7333	−0.5417	0.4802	0.3962
TiO_2					1.0000	0.7748	0.6314	0.7422	−0.4371	0.6126	0.5787
Fe_2O_3						1.0000	0.6152	0.6261	−0.5302	0.5468	0.1941
K_2O							1.0000	0.8477	−0.4461	0.4692	0.5120
SIO_2								1.0000	−0.4208	0.5588	0.4939
MnO									1.0000	−0.1436	−0.0772
MgO										1.0000	0.4112
Na_2O											1.0000

Significant correlation between Si, Al, Ti, K and Fe was found. These elements are mainly concentrated in the clastic matrix of the concretions and are grouped into the "clastic" group. P, Ca, total REEs and Y also show significant correlation and they conform the "authigenic" group.

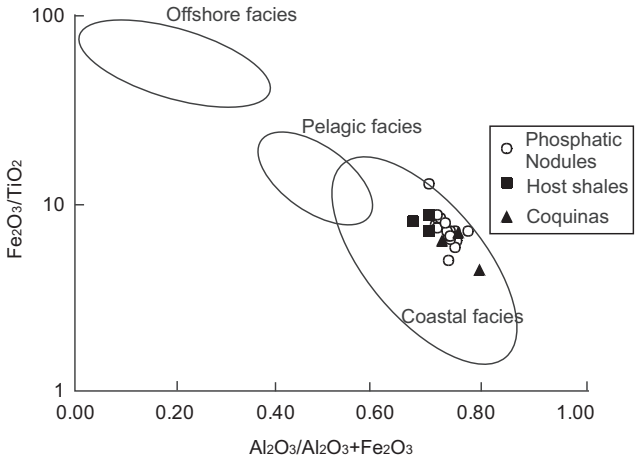

Fig. 6. Plot of Fe_2O_3/TiO_2 vs. $Al_2O_3/Al_2O_3+Fe_2O_3$ in coquinas (triangles), shales (squares) and concretions (circles) from the Gaiman Formation. All the samples are tightly grouped indicating the same detrital source for concretions, host shales, and coquinas. The three fields, offshore, pelagic and coastal defined by Murray (1994) for modern seafloor cherts are shown.

Ce anomaly vs. Y anomaly and Ce anomaly vs. La/Nd ratio in phosphatic samples (Figs. 8A and B, respectively) show little correlation. The same is true for Y anomaly and La/Nd ratio vs. total REEs (Figs. 8C and D, respectively). On the other hand, Y anomaly vs. La/Nd (Fig. 8E) shows a positive correlation.

4.4. Factor analysis

Three factors can account for the main variance of the system in the principal component analysis (Table 4, Figs. 9A and B). Factor 1 represents the variance linked to major components that are clustered by their loading values into two well-defined groups: (a) SiO_2, Al_2O_3, TiO_2, K_2O, Na_2O, MgO and Fe_2O_3; (b) CaO, P_2O_5, and total REEs and Y. Factor 2 loadings can be attributed to yttrium and cerium anomalies, and the La/Nd ratio. Factor 3 shows MnO as the only variable which has a significant loading.

5. Discussion

5.1. Depositional and diagenetic environment of the Gaiman Fm.

Lower Miocene beds of Gaiman Fm. were accumulated in offshore to shoreface environments in a shallow, storm-dominated shelf (Scasso and Castro, 1999), which extended several hundreds of kilometre to the east up to the South Atlantic slope. Abundant fossil remains and strong bioturbation throughout the unit suggest intense biological activity in the water column and at the well-oxygenated sea bottom. The horizontal, undeformed beds of Gaiman Fm. never underwent deep burial in the study area, with the maximum estimated overburden between 100 and 200 m. Therefore, burial and high temperature diagenetic processes can be ruled out. Early-diagenetic processes, however, caused big changes in sediment components. Scasso and Castro (1999) suggested an early-diagenetic origin for the phosphatic concretions, based on the phosphatic ooids in some levels of the Gaiman Fm. and on the fact that concretions were already formed when slight intrabasinal

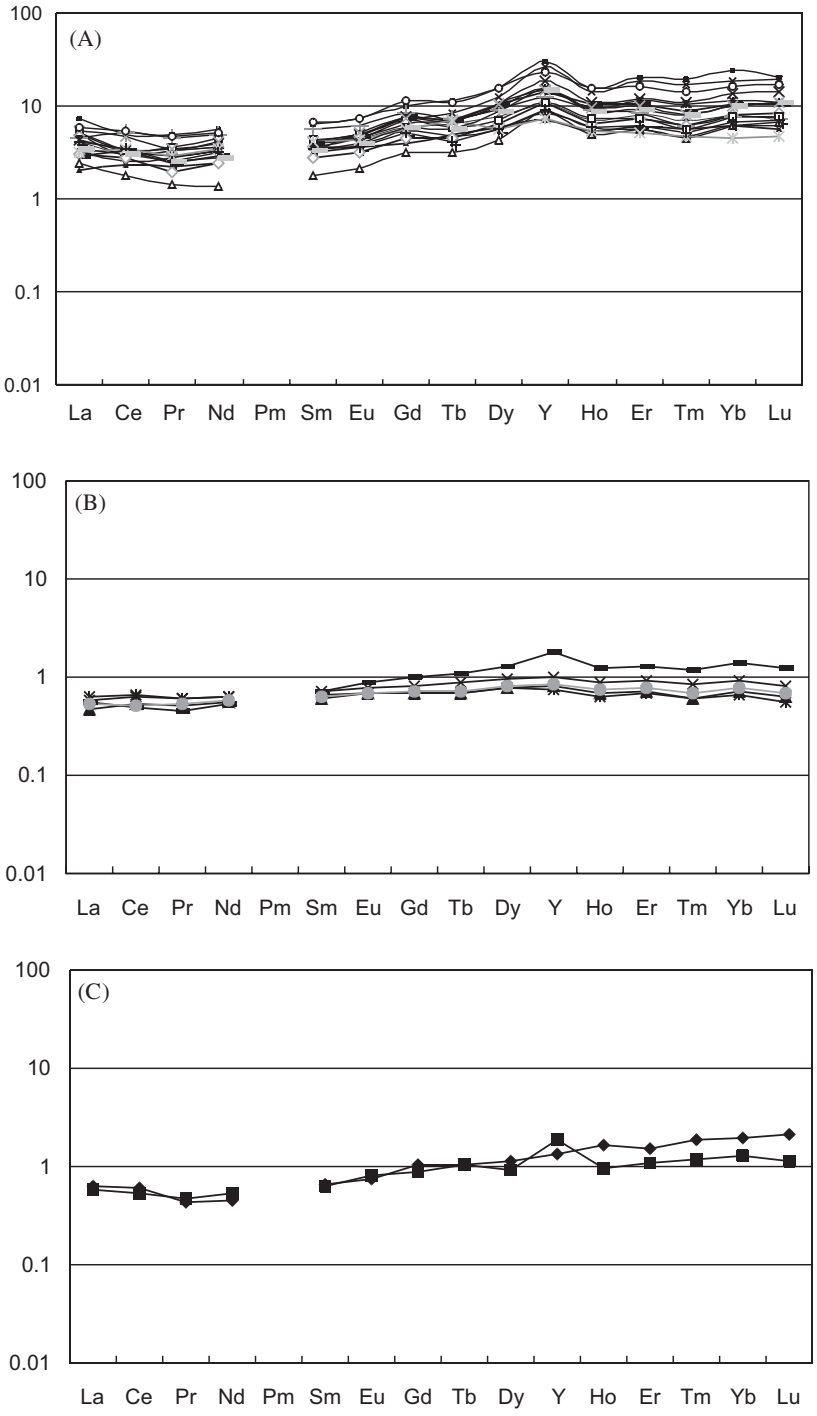

Fig. 7. Shale normalized REE distribution for (A) concretions, (B) host shales, and (C) coquinas from the Gaiman Formation. Values were normalized to Piper shale reference material (Piper, 1974). Phosphatic concretions (A) show a pattern depleted in light REEs and enriched in heavy REEs in comparison to shales, with a weak negative Ce anomaly. Host shales (B) exhibit a typical flat pattern with total REE contents slightly lower than Piper reference shale. Coquinas (C), containing up to 5% P_2O_5 from reworked concretions display a pattern similar to concretions, but lower total REEs.

erosion of the sea bottom mechanically concentrated them. Good preservation of fossils and delicate components like pumice and shards, with empty or partially filled pores and glass vesicles in the concretions (Figs. 4 and 5) also support the early precipitation of phosphate, before incipient compaction took place. Furthermore, phosphate removed by infaunal organisms before complete crystallization occurred (Fig. 2) indicates that phosphate concretions were developed at the initial

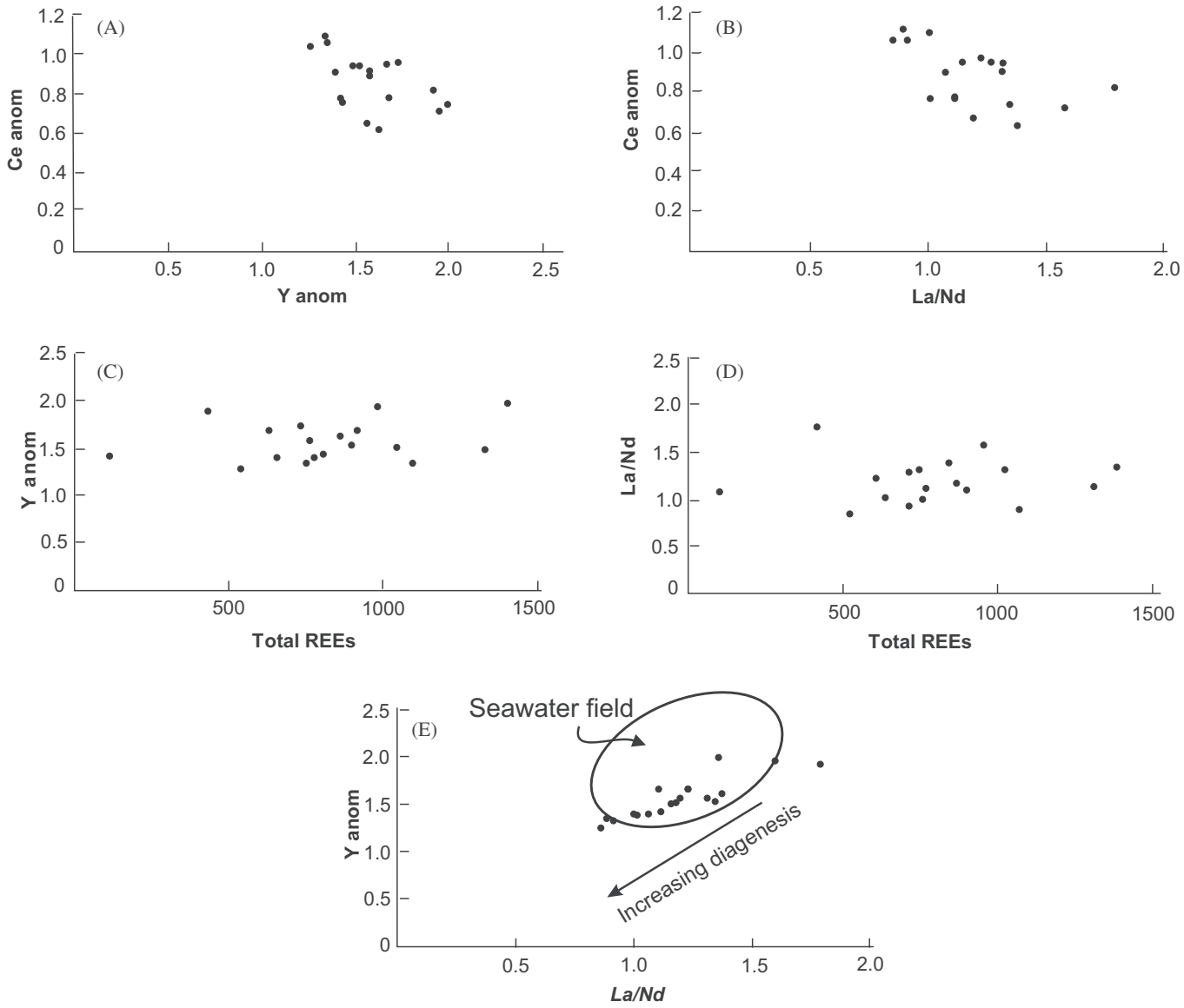

Fig. 8. (A and B) Ce anomaly vs. Y anomaly and Ce anomaly vs. La/Nd anomaly show little correlation, presumably as a result of redox Ce recycling. (C and D) Y anomaly vs. total REEs and La/Nd vs. total REEs also display poor correlation. Y anomaly vs. La/Nd (E) show positive correlation as pointed out by Shields and Stille (2002) suggesting that Y has the same behavior of La in pore waters.

stages of the early diagenesis, before the sediment was buried beyond the reach of the mega-infauna, no deeper than 2–3 m below the sea bottom. Molluscan molds of dissolved calcareous shells suggest cold and corrosive marine and/or early-diagenetic pore waters. Mn and Fe concretions and oxidized horizons, as well as silicified and more rarely gypsified oyster levels, suggest a chemically active diagenesis.

A remarkable stratigraphic association of densely bioturbated levels dominated by *Ophiomorpha* isp. overlain by zones with phosphatic concretions rich in claws of *Callianasa* sp., a Thalassinidean shrimp, was found by Scasso and Castro (1999) and Scasso et al. (2004) who assumed a genetic link for the *Ophiomorpha*—phosphate—condensed bed association via enhanced water circulation between the sea bottom and the sediments, mainly through the large *Ophiomorpha* shafts (Figs. 2 and 9).

5.2. Geochemical characteristics of Gaiman phosphatic concretions

Phosphatic concretions from several localities and from different stratigraphic parts of the Gaiman Fm. show closely similar major and REE

Table 4
Extraction of factors by principal components analysis from the set of measured variables in Gaiman Fm. concretions: three factors account for the 73% of variance

Eigenvalues

Extraction: Principal factors (comm. = multiple *R*-square)

	Eigenval	% Total variance	Cumul. eigenval	Cumul. %
1	8.282	55.214	8.282	55.214
2	1.802	12.013	10.084	67.227
3	0.897	5.983	10.981	73.210

Factory loadings

Variable	Factor 1	Factor 2	Factor 3
ΣREEs	−0.79825	0.14681	0.32194
Y	−0.74771	0.40435	0.35877
Y anomaly	−0.69649	0.62794	−0.10915
La/Nd	−0.38629	0.78800	−0.23451
Ce anomaly	−0.44431	−0.44356	0.08745
CaO	−0.96069	−0.15494	0.01560
P_2O_5	−0.92568	−0.09456	−0.04951
Al_2O_3	0.88105	0.18331	0.15801
TiO_2	0.82139	0.28028	−0.02692
Fe_2O_3	0.79237	0.19847	0.22100
K_2O	0.86715	0.09768	0.08869
SiO_2	0.91094	0.10679	0.01511
MnO	−0.44987	−0.30271	−0.55457
MgO	0.60802	0.22835	−0.29843
Na_2O	0.49158	0.23594	−0.32955

Summary of the analysis showing the eigenvalues with their associated percent of total variance, cumulative eigenvalues and cumulative percent of variance is shown on top. The eigenvalues are arranged in decreasing order of importance of the respective factors in data variation. Below: Factor loading of the variables on each factor. Al_2O_3, TiO_2, Fe_2O_3, K_2O and SiO_2 (mostly in clastic components) have significant and positive loading on Factor 1, CaO, P_2O_5, Y and total REEs (mainly in authigenic minerals) have significant but negative loading on Factor 1. Y anomaly and La/Nd and minor Ce anomaly (all associated to fractionation in pore waters) have significant values in Factor 2, and only MnO has significant loading in Factor 3, pointing out the variance accounted by its mobility in the marine environment.

compositions (Fig. 7A). As a consequence, it is assumed that they all result from similar geochemical processes that, according to the petrographical textures in the concretions, occurred shortly after sedimentation.

5.2.1. *Major elements*

Two groups of oxides are clearly defined in the correlation matrix of Table 3 (see also Figs. 9A and B). The first, called the "clastic" group, is formed by oxides of Si, Al, Ti, K, Mg, Na and Fe dominant in the aluminosilicates that make up the terrigenous-clastic fraction; the second, called the "authigenic" group, is formed by P, Ca, and total REEs oxides, dominant in the authigenic minerals phases. As it is shown in Figs. 4 and 5, authigenic phosphate precipitated in the pores of the original clastic fraction composed of quartz, feldspar, pyroxene, pumice, glass shards, and other components. Iron does not exhibit a good correlation with phosphorus, calcium or total REEs (Table 3). Instead, the correlation coefficients of iron with Ti, Al, Si and K indicate that Fe mainly comes from aluminosilicates of terrigenous origin. A plot of Fe_2O_3/TiO_2 vs. $Al_2O_3/Al_2O_3 + Fe_2O_3$, after Murray (1994) shows the Gaiman Fm. samples from different lithologies tightly grouped, indicating the similar composition of the clastic fraction in all the samples (Fig. 6). Analyses of major elements from modern seafloor cherts can distinguish different fields for pelagic, offshore and coastal sediments using major oxides ratios of elements relatively unaffected by postdepositional process, like Fe_2O_3, TiO_2, Al_2O_3 and Fe_2O_3 (Murray, 1994). As shown in Fig. 6, the Gaiman Fm. samples consistently fall within the continental margin field, indicating a common clastic source for concretions, host shales, and coquinas.

Manganese oxide shows a weak correlation to either the "clastic" or "authigenic" oxides (Table 3). Correlation between Mn and Fe is not evident, although these elements normally have similar redox behavior. Thus, Mn shows a distinctive behavior in the Gaiman Fm. samples, which cannot be compared to any other major element. Mn oxihydroxides are proposed to be carriers of REEs, influencing their partitioning in seawater (Moffett, 1990; Moffett, 1994; Sholkovitz et al., 1994). However, recent work has suggested that Mn is not the main scavenger of REEs in seawater (Sholkovitz et al., 1992; Haley and Klinkhammer, 2002; Haley et al., 2004). Accordingly, Mn shows no correlation to REEs in the Gaiman Fm. phosphates and the results of factor analysis indicate that MnO is the only variable that has a significant loading in Factor 3. Many authors have documented the mobility of Mn in marine sediments (Bonatti, 1971; Marchig and Reyss, 1984; Murray, 1994; Namerof et al., 2002) and we assume that high mobility of Mn in the marine environment is the main reason for its particular behavior in Gaiman concretions.

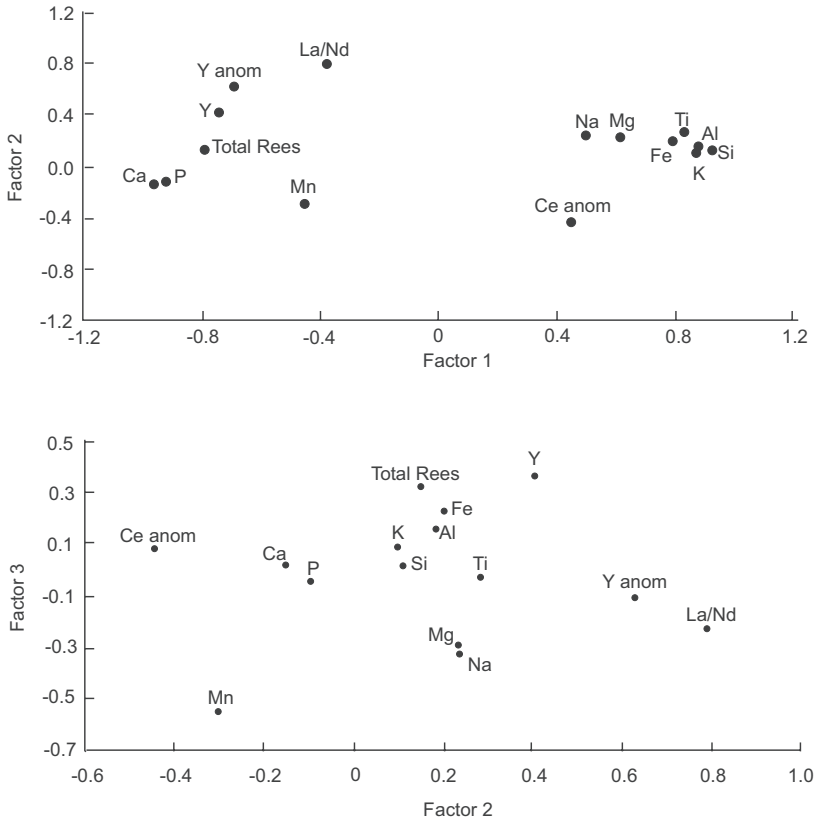

Fig. 9. Factor analysis: Three factors take into account the main variance of the system in the principal components analyses (see Table 4). (A) Plot of Factor 1 vs. Factor 2, and (B) Plot of Factor 3 vs. Factor 2. Factor 1 represents oxide loading values clustered in two groups of opposite sign: the clastic group with Si, Al, Ti, K and Fe and the authigenic group with P, Ca, total REEs and Y. Factor 2 shows significant loading in Y anomaly, La/Nd ratio and Ce anomaly, probably linked to minor compositional changes in REEs into the diagenetic environment. In Factor 3, MnO is the only variable which has a significant loading, probably because of the high mobility of MnO in pore waters.

5.2.2. *REEs and Yttrium*

REEs are scavenged through the seawater column as a result of the action of carriers such as organic matter and oxihydroxides. They form particulates together with terrigenous materials and precipitate on the sea bottom. The greater stability of the HREE complexes in solution (Cantrell and Byrne, 1987) together with the higher adsorption of LREEs in particulate matter (Byrne and Kim, 1993), make up the characteristic seawater pattern of these elements in the oceans, which typically shows HREE enrichment and a varied Ce anomaly. A significant negative Ce anomaly is typical in deep, oxygenated marine waters. Its formation depends on factors like depth, stratification and biological activity of the basin. Oxygenated pore waters in the bottom sediments also may display negative Ce anomalies, which can be suppressed as Ce^{3+} from the organic complexes is released into solution (Haley et al., 2004).

Gaiman Fm. concretions show the general depletion of LREEs broadly typical of the seawater pattern, and an apparent weak negative Ce anomaly in both reworked and unreworked phosphatic concretions, qualitatively described here as the "V" defined by La, Ce and Pr. This anomaly, however, can be an artifact of La enrichment with Pr anomaly ~1, as pointed out by Bau et al. (1996) and Shields and Stille (2002).

Many authors agree that REEs are incorporated into authigenic phosphate without fractionation, keeping the original water pattern, but diagenetic processes, especially recrystallization, may induce later differentiation (Shields and Stille, 2002; Reynard et al., 1999; Kidder et al., 2003). On the other hand, the light-REEs depletion may be interpreted as a weathering influence (Kidder and Eddy-Dilek, 1994). The Gaiman Fm. did not undergo diagenesis strong enough to cause complete recrystallization of the phosphate. In addition, we

assume that weathering effects are negligible in the REE pattern of the concretions, because we have found the same pattern in recently-exposed fresh concretions from coastal cliffs as well as in other externally oxidized and more altered concretions. Thus, we assume that the REE pattern in Gaiman samples is the result of primary phosphatic precipitation from seawater or pore water in the sediments during early diagenesis. Gaiman Fm. sediments accumulated in shallow water, at different depths related to eustatic changes in the sea level. However, the REE patterns in the concretions

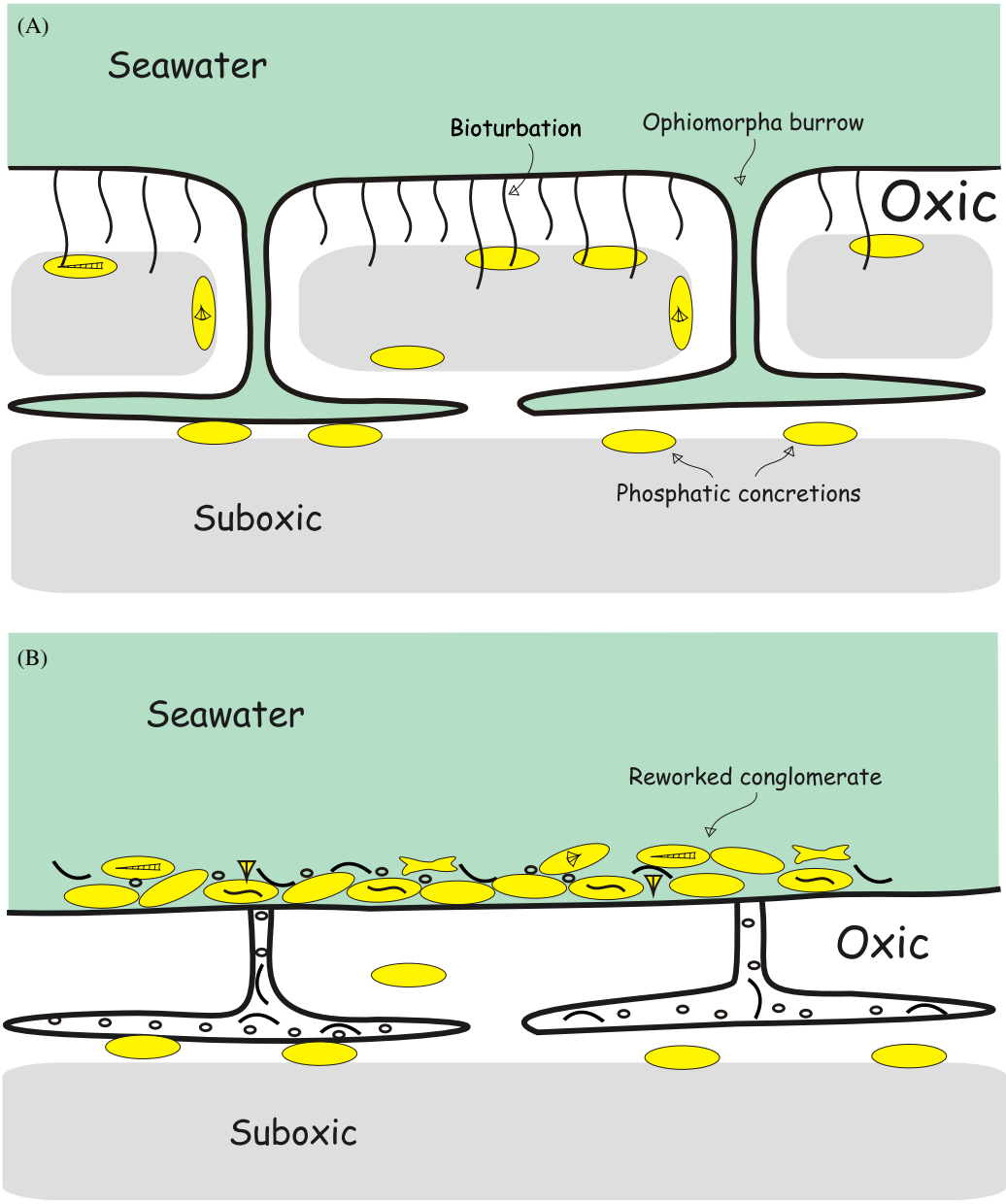

Fig. 10. (A) Sedimentary-diagenetic system at the sea bottom during formation of concretions in the Gaiman Formation. 7 cm wide, vertical or slightly inclined *Ophiomorpha* shafts penetrate up to 3 m deep into the substrate, where they are connected to a main network of burrows. The burrow network enhanced water circulation between the sea bottom and the sediments, affecting oxygenation, ion diffusion and pore water renewal. Therefore oxic and suboxic diagenetic zones will reach deeper parts of the sediment, and an extended oxic-suboxic zone will develop along the burrows, favouring the formation of phosphatic concretions. In addition, organic matter decaying in the burrows might create locally anoxic or suboxic microenvironments, and sediment mixing and reworking by organisms will allow the early-diagenetic reagents to be fully in contact. (B) Formation of reworked beds after erosion of the sea bottom, winnowing and reworking of the concretions. Conglomerates are rich in fossil-or-burrow-nucleated concretions, marine vertebrate bones and shark teeth. Modified from Scasso and Castro (1999) and Scasso et al. (2004).

are always the same, suggesting that they are not related to the original depth of sediment accumulation (Fig. 10).

Phosphate precipitation, organic matter and biological activity are known to be strongly related. Felitzyn and Morad (2002) found a direct correlation between the REEs patterns of biogenic phosphate and organic debris. Signals of the decay of the organic matter, like humic acids and kerogen, are not preserved in the Gaiman Fm., precluding their REEs analysis. However, REE patterns of Gaiman concretions compare well with "linear" REE patterns of Haley et al. (2004) related to the rate or degradation of organic complexes (Fig. 11). This pattern may be present in oxic to anoxic environments, but only appears near the sediment surface where pore waters are oxic to suboxic, as a result of remineralization of the organic complexes. The linear patter can be found together with other different patterns like the "HREE enriched" or the "MREE bulge" patterns in pore waters within a few decimeters below the sea bottom, when redox conditions change. On the other hand, the Ce^{4+} present as oxihydroxide in particulate matter close to the seafloor changes to Ce^{3+} into solution if the environment becomes more reducing. This results in an increased availability of cerium, which is then incorporated into the phosphate minerals through adsorption or substitution mechanisms (Reynard et al., 1999) and therefore produces a reduced Ce anomaly. Thus the linear pattern common to all concretions in Gaiman Fm. suggests that they have formed in the same diagenetic conditions, most likely precipitated from oxic to suboxic early-diagenetic pore waters.

5.2.3. Other anomalies and REE ratios

The Y anomaly and La/Nd ratio can be useful indicators of postdepositional changes related to variations in the composition of circulating fluids. Both elements have positive anomalies in seawater (Zhang et al., 1994; Bau et al., 1996), and they are not affected by environmental redox changes, but in the sediments these anomalies might decrease with increasing diagenesis, as remobilization by exchange with pore fluids take place (Shields and Stille, 2002).

Positive Y anomaly and La/Nd ratios are commonly found in particulate matter (Bau et al., 1996), but Y and La are less effectively scavenged than their respective neighbors in the ReeY (REEs plus Y) series. As a result, anomalies in Y and La/Nd ratio are lower in particulate matter than in seawater. Bau et al. (1996) assigned the special behavior of Y and La to their more stable electronic configuration, similar to noble gases, with half filled 4f orbital, known as the tetrad effect.

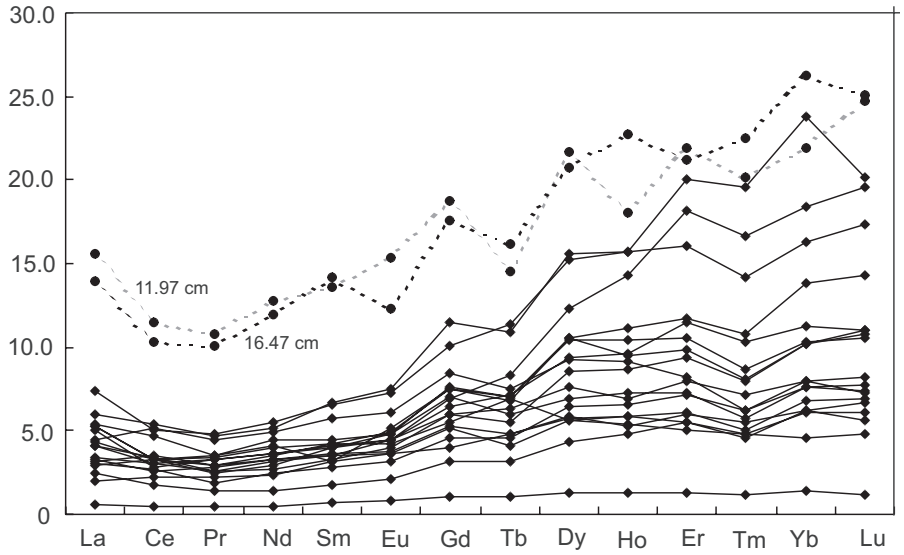

Fig. 11. Two pore-water REE patterns 11.97 and 16.47 cm below the sea bottom (dotted lines) from suboxic, iron free, early-diagenetic environment (locality Sta. 9 from Haley et al., 2004) compared to the REE patterns of Gaiman Formation concretions. Good correlation between both suggests that concretions precipitated quantitatively from this type of pore water, thus inheriting a flat REE pattern as a consequence of LREEs being released from organic matter decay. All the samples were normalized to Piper's shale, but values from pore water were multiplied by an appropriate factor scale for better visualization.

Shields and Stille (2002) indicated values between 1.5 and 2.3 for Y anomaly and 0.8–1.3 for La/Nd ratio in modern seawater. Yttrium anomaly in Gaiman Fm. concretions is low and shows a positive correlation with La/Nd ratio, suggesting that Y and La behave in the same way in pore waters. Most values found in the Gaiman Fm. concretions are equivalent to those of seawater or slightly lower (Fig. 8E), indicating that Gaiman Fm. concretions did not undergo intense diagenesis (Shields and Stille, 2002). Instead, they were probably formed from phosphatic solutions impoverished in Y and La in relation to other REEs, as a result of REEs release to solution from organic complexes in the early diagenesis. Y and Ce anomalies and La/Nd ratio in Gaiman Fm. concretions have significant loadings in Factor 2 (Figs. 9A and B) that point out a secondary variability of the system, probably linked to minor compositional changes in REEs in the diagenetic environment. The lack of correlation between Ce anomaly vs. Y anomaly, and Ce anomaly vs. La/Nd (Figs. 8A and B) is probably due to redox Ce recycling. In the sediments, just a few centimeters below the sea bottom, REEs can be released by organic matter remineralization, and pore water acquires a flatter REE pattern and a lower La/Nd ratio than those of the seawater (Shields and Stille, 2002; Haley et al., 2004). Gaiman Fm. concretions presumably formed in that environment, similarly show flat REE patterns (Fig. 11) and low La/Nd ratios (Fig. 8E).

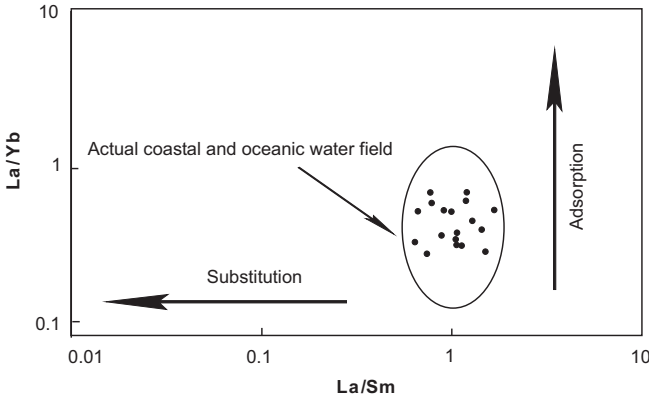

Fig. 12. La/Yb ratio vs. La/Sm ratio for Gaiman Formation concretions. Values are similar to those of modern coastal and oceanic waters provided by Reynard et al. (1999) indicating that REEs in concretions mostly preserved the original seawater values. Concretions apparently did not undergo strong postdepositional recrystallization, that would have shifted the values along the "substitution" horizontal arrow, nor intense adsorption, that would have caused value shifting along the vertical "adsorption" arrow.

The La/Yb ratio varies between 0.2 and 0.7, and the La/Sm ratio between 0.75 and 1.68 in Gaiman Fm. concretions (Fig. 12). These values are similar to those of modern oceanic water values provided by Reynard et al. (1999), which are fairly homogeneous (0.2–0.5 for La/Yb and 0.6–1.6 for La/Sm). The La/Yb and La/Sm ratios are considered as indicators of light REE enrichment and bell-shaped patterns, respectively (Reynard et al., 1999). These authors studied the crystal chemical factors that can influence the REE fractionation between apatite and water. They pointed out that if the adsorption of REEs onto authigenic apatite was the main fractionation mechanism, La/Yb values would increase in comparison to seawater, due to the preferential sorption of LREEs, but no significant changes should be observed in La/Sm. On the contrary, if substitution by recrystallization was the main process in the REE incorporation to the apatite lattice, the La/Sm ratio would show a significant decrease and a "bell-shaped" pattern would be observed. Thus, according to Reynard et al. (1999) REEs could be incorporated: (a) quantitatively from seawater without fractionation; (b) by adsorption in moderate diagenesis; or (c) by recrystallization in more pronounced diagenesis.

The La/Yb and the La/Sm ratios in Gaiman Fm. concretions (Fig. 12) plot into the field of oceanic water of Reynard et al. (1999) indicating that REEs were incorporated preserving the seawater pattern and that neither strong postdepositional recrystallization nor strong adsorption took place in them.

5.3. *Geochemical insights in the phosphogenetic system*

The REEs geochemical signatures and the sedimentological features indicate that Gaiman Fm. concretions did not undergo strong diagenesis or weathering. Their relatively flat pattern could not be inherited from the associated detritic sediments because concretions show high-REE enrichment relative to host shale (Fig. 3). Flat, "linear" REE patterns like that of the Gaiman phosphatic concretions are typical from oxic or suboxic pore waters in surficial sediments (Haley et al., 2004). According to these authors, organic coatings formed in the surface seawater are enriched in LREEs and Ce. The fraction of organic coatings that reach the sea bottom is remineralized, driving a rapid increase in REE concentration, at or a few cm below the sea bottom. Differential release of LREEs

and Ce in oxic or suboxic early-diagenetic environments returns the REE ratio to flat patterns resembling the original patterns at the sea surface. Thus, quantitative precipitation of REE minerals from pore water in the Gaiman Fm. will reproduce the flat pattern typical of oxic–suboxic pore waters. On the other hand phosphate precipitation mainly takes place in suboxic conditions (Jarvis et al., 1994) and reactions involved in "redox pumping of iron" (Froelich et al., 1988) and other phosphogenetic mechanisms are related to redox changes with depth into the sediment. A sediment mixed layer up to 15 or 20 cm below the sea bottom, probably resulting from bioturbation, was considered critical for the redox cycling of iron and phosphorite formation on the East Australian continental margin (O'Brien et al., 1990). Sediment mixing and reworking by organisms favored early-diagenetic processes in the Gaiman Fm., allowing the reagents to be fully in contact. Phosphatic concretions around fossils suggest that decaying organic matter from the soft parts of the organisms created suboxic microenvironments prone to phosphate precipitation (Fig. 2C). Enhanced water circulation through a dense network of tunnels and shafts of *Ophiomorpha* isp. and smaller burrows improved ion diffusion and pore water renewal in the early-diagenetic system of the Gaiman Fm. As a consequence, many concretions were formed around and along the walls of the big burrows or within them (Figs. 2 and 10). Anoxia can be reached a few centimeters below the sea bottom in normal marine conditions, but in the Gaiman Fm. concretions formed throughout an extended oxic–suboxic zone as a result of deeper penetration of oxigenated sea bottom waters in the sediments, improving the pore water oxigenation and turning oxic or suboxic the otherwise anoxic deeper parts of the sediments. Phosphogenesis processes take place at very shallow burial and were therefore constrained to the oxic–suboxic zone. As a result, all the concretions in the unit show the same REE pattern.

6. Conclusions

The Gaiman Fm. phosphatic concretions show similar major element ratios, REE patterns and total REE contents in different stratigraphic levels and geographic locations suggesting a common process for their origin.

Major elements oxides in phosphatic concretions are grouped into two well-defined sets: the "clastic" group (Si, Al, Ti, K and Fe), which corresponds to the clastic fraction of the samples, mainly composed by quartz, feldspar, biotite, pyroxene, glass and clay minerals, and the "authigenic" group (P, Ca and total REEs), which corresponds to the authigenic cements of francolite and calcite. Manganese has a different behavior, most likely to its high mobility in seawater. Major element ratios indicate that the composition of the shales and host rocks is similar to the clastic fraction within the concretions.

Shale-normalized REE patterns from phosphatic concretions are slightly depleted in LREEs and slightly enriched in HREEs in comparison to shales. All phosphate concretions display a weak negative Ce anomaly and no differences between *in situ* and reworked concretions were found. Host shales exhibit a typically flat REE pattern and the presence of reworked concretions impart to the coquinas a "concretion-like pattern" with lower total REE contents.

The La/Yb and the La/Sm ratios in Gaiman Fm. concretions indicate that the REEs incorporation process preserved the seawater pattern and that neither strong postdepositional recrystallization nor strong adsorption took place.

The Y anomaly and La/Nd ratios in Gaiman Fm. concretions are equivalent to seawater or slightly lower, also pointing out that Gaiman concretions did not undergo intense diagenesis, but were probably formed from phosphatic solutions impoverished in Y and La in relation to other REEs, as a result of REEs release to solution from organic complexes in the early diagenesis.

Water circulation through burrows at the Miocene seawater–sediment interface improved ion diffusion and pore water renewal in the sediments, allowing the development of a widened oxic–suboxic zone. In addition, sediment mixing and reworking by organisms and microenvironments from organic matter decay within fossils and burrows contributed to phosphatic concretion formation.

REE patterns in early-diagenetic concretions of the Gaiman Fm. suggest quantitative precipitation from early-diagenetic pore waters, reproducing the flat pattern of oxic–suboxic recent pore waters, which result from remineralization of organic coatings rich in Ce and other LREEs.

Acknowledgements

Financial support for this study was provided by the University of Buenos Aires (UBACYT EX081)

and by CONICET (PIP 02343). The Comisión Nacional de Energía Atómica is acknowledged for providing access to the ICP–AES equipment.

References

Altschuler, Z.S., Berman, S., Cuttiti, F., 1967. Rare earths in phosphorites-geochemistry and potential recovery. US Geological. Survey. Professional Paper 575B, B1–B9.

Altschuler, Z.S., 1980. The geochemistry of trace metals in marine phosphorites: Part 1. Characteristic abundances and enrichment. In: Bentor, Y.K. (Ed.), Marine Phosphorites. Society for Economic and Paleontologist and Mineralogists, vol. 29. The Society of Sedimentary Geology, Oklahoma, USA, pp. 19–30.

Bau, M., Koschinsky, A., Dulski, P., Hein, J.R., 1996. Comparison of the partitioning behaviours of yttrium, rare earth elements, and titanium between hydrogenetic marine ferromanganese crusts and seawater. Geochimica et Cosmochimica Acta 60, 1709–1725.

Bonatti, E., 1971. Manganese fluctuation in Caribbean sediment cores due to post-depositional remobilization. Bulletin of Marine Science 21, 510–518.

Byrne, R.H., Kim, K., 1993. Rare earth precipitation and coprecipitation behavior: the limiting role of PO_4^{-3} on dissolved rare earth concentrations in seawater. Geochimica et Cosmochimica Acta 57, 519–526.

Cantrell, K.J., Byrne, R.H., 1987. Rare earth element complexation by carbonate and oxalate ions. Geochimica Cosmochimica. Acta 51, 597–605.

Castro, L.N., Fazio, A.M., 2004. Rare-earth elements signature of patagonian marine sedimentary phosphates, Argentina International Symposium on the Geology and Geophysics of the Southernmost Andes, the Scotia Arc and Antarctic Peninsula, Buenos Aires International Journal of Earth Science; Bolletino de Geofisica 45: Session 7; Sedimentary Process, pp. 177–179.

Castro, L.N., Scasso, R.A., Fazio, A.M., 2000. Rare earths in phosphate deposits in Patagonia, 31 International Geological Congress. Rio de Janeiro. In: Symposia Sedimentology 3.5. Authigenic minerals in marine and continental environment. CD abstract Ind. 231.

Elderfield, H., Greaves, M.J., 1982. The rare earth elements in seawater. Nature 296, 214–219.

Elderfield, H., Hawkesworth, C., Greaves, M., Calvert, S., 1981. Rare earth elements geochemistry of oceanic ferromanganese nodules and associated sediments. Geochimica et Cosmochimica Acta 45, 513–528.

Felitzyn, S., Morad, S., 2002. REEs patterns in latest Neoproterozoic-early Cambrian phosphate concretions and associated organic matter. Chemical Geology 187, 257–265.

Froelich, P., Arthur, M.A., Burnett, W.C., Deakin, M., Hensley, V., Jahnke, R., Kaul, L., Kim, K., Roe, K., Soutar, A., Vathakanon, C., 1988. Early diagenesis of organic matter in Perú continental margin sediments: phosphorites precipitation. Marine Geology 80, 309–343.

Glenn, C.R., Follmi, K.B., Riggs, S.R., Baturin, G.N., Grimm, K.A., Trappe, J., Abed, A.M., Galli-Olivier, C., Garrison, R.E., Ilyin, A.V., Jehl, C., Rohrlih, V., Sadaqah, R.M.Y., Schidlowski, M., Sheldon, R.E., Siegmund, H., 1994. Phosphorus and phosphorites: sedimentology and environments of formation. Eclogae Geologicae Helvetiae. Journal of Swiss Geological Society 87 (3), 747–788.

Goldberg, E.D., Kodie, M., Schmiyy, R.A., Smith, H.V., 1963. Rare earth distribution in marine environment. Journal of Geophysical Research 68, 4207–4209.

Haley, B.A., Klinkhammer, G.P., 2002. Development of a flow through system for cleaning and dissolving foraminiferal tests. Chemical Geology. 185, 51–69.

Haley, B., Klinkhammer, G.P., McManus, J., 2004. Rare earth elements in pore waters of marine sediments. Geochimica et Cosmochimica Acta 68 (6), 1265–1279.

Jarvis, I., Burnett, W.C., Nathan, Y., Almbaydin, F.S.M., Attia, A.K.M., Castro, L.N., Flicoteaux, R., Hilmy, M.E., Husain, V., Qutawnah, A.A., Serjani, A., Zanin, Y.N., 1994. Phosphorite geochemistry: state-of-the-art and environmental concerns. Eclogae Geologicae Helvetiae Journal of Swiss Geological Society 87 (3), 643–700.

Kidder, D.L., Eddy-Dilek, C.A., 1994. Rare-earth element variation in phosphate nodules from midcontinent Pennsylvanian cyclothems. Journal of Sedimentary Research. A 64, 584–592.

Kidder, D., Krishnaswamy, P., Mapes, P., 2003. Elemental mobility in phosphatic shales during concretion growth and implications for provenance analysis. Chemical Geology 198, 335–353.

Kolodny, Y., 1981. Phosphorites in the sea. In: Emiliani, C. (Ed.), vol. 7, Willey Interscience, New York, pp. 981–1023.

Leanza, H.A., Spiegelman, A.T., Hugo, C.A., 1981. Manifestaciones fosfáticas de la Formación Patagonia: su génesis y relación con el vulcanismo piroclástico-silíceo. Revista de la Asociación Argentina de Mineralogía Petrología y Sedimentología 11, 1–12.

Marchig, V., Reyss, J.L., 1984. Diagenetic mobilization of manganese in Peru basin sediments. Geochimica et Cosmochimica Acta 48, 1349–1352.

McArthur, J.M., Walsh, J.N., 1984. Rare-earth geochemistry of phosphorites. Chemical Geology 47, 191–220.

McLennan, S.M., 1989. Rare earth elements in sedimentary rocks: influence of provenance and sedimentary processes. In: Lipin, B.R., McKay, G.A. (Eds.), Geochemistry and Mineralogy of Rare Earth Elements. Reviews in Mineralogy 21, pp. 169–200.

Moffett, W., 1990. Microbially mediated cerium oxidation in seawater. Nature 345, 421–423.

Moffett, W., 1994. A radiotracer study of cerium and manganese uptake onto suspended particles in Chesapeake Bay. Geochimica et Cosmochimica Acta 58, 695–703.

Murray, R.W., 1994. Chemical criteria to identify the depositional environment of chert: general principles and applications. Sedimentary Geology 90, 213–232.

Namerof, T.J., Balistrieri, L.S., Murray, J.M., 2002. Suboxic trace metal geochemistry in the eastern tropical North Pacific. Geochimica et Cosmochimica Acta 66 (7), 1139–1158.

O'brien, G.W., Milnes, A.R., Veeh, H.H., Heggie, D.T., Riggs, S.R., Cullen, D.J., Marshall, J.F., Cook, P.J., 1990. Sedimentation dynamics and redox iron-cycling: controlling factors for the apatite-glauconite association on the East Australian continental margin. In: Notholt, A.J.G., Jarvis, I. (Eds.), Phosphorite Research and Development, 52. Geological Society Special Publication, pp. 61–86.

Piper, D.Z., 1974. Rare earth elements in the sedimentary cycle: a summary. Chemical Geology 14, 285–304.

Reynard, B., Lécuyer, C., Grandjean, P., 1999. Crystal-chemical controls on rare-earth element concentrations in fossil biogenic apatites and implications for paleoenvironmental reconstructions. Chemical Geology 155, 233–241.

Scasso, R.A., Castro, L.N., 1999. Cenozoic phosphatic deposits in North Patagonia, Argentina phosphogenesis, sequence-stratigraphic and paleoceanographic meaning. Journal of South American Earth Sciences 12, 471–487.

Scasso, R.A., Castro, L.N., Fazio, A.M., 2004. Genetic relationship between bioturbation and phosphogenesis in shallow marine environment. ICHNIA, In: First International Congress on Ichnology, Abstracts, Trelew, Chubut, 75pp.

Shapiro, L., 1975. Rapid analysis of silicate, carbonate and phosphate rocks. Geological Survey Bulletin 1401, 76.

Shields, G., Stille, P., 2002. Diagenetic constraints on the use of cerium anomalies as palaeoseawater redox proxies: an isotopic and REE study of Cambrian phosphorites. Chemical Geology 175, 29–48.

Sholkovitz, E.R., Landing, W.M., Lewis, B.L., 1994. Ocean particle chemistry: the fractionation of rare earth elements between suspended particles and seawater. Geochimica. Cosmochimica Acta 58, 1567–1579.

Sholkovitz, E.R., Shaw, T.J., Schneider, D.L., 1992. The geochemistry of rare earth elements in the seasonally anoxic water column and porewaters of Chesapeake Bay. Geochimica Cosmochimica Acta 56, 3389–3402.

Zhang, J., Amakawa, H., Nosaky, Y., 1994. The comparative behavior of Y and lanthanides in seawater on the North Pacific. Geophysic Resources Letter 21, 2677–2680.